

The power balancing benefits of wave energy converters in offshore wind-wave farms with energy storage[☆]

Jocelyn M. Kluger ^{a,*¹}, Maha N. Haji ^{b,1}, Alexander H. Slocum ^a

^a Department of Mechanical Engineering, Massachusetts Institute of Technology, Cambridge, MA, United States of America

^b Sibley School of Mechanical and Aerospace Engineering, Cornell University, Ithaca, NY, United States of America

ARTICLE INFO

Keywords:

Offshore wind energy
Wave energy
Compressed air energy storage
Supply–demand matching
Optimization
Cost analysis

ABSTRACT

With many countries planning to significantly increase grid renewable energy penetration levels, we consider the role of wave energy in supply–demand matching. We investigate how incorporating wave power into an offshore wind farm affects farm power predictability, smoothness, required energy storage capacity, and cost. In this paper, we do a first-order cost analysis of an offshore farm comprised of floating wind turbines and wave energy converters that are both standalone and combined and onshore compressed air energy storage. Then, we do a parameter sweep investigation of an isolated power network supplied by varied grid renewable energy penetration levels supplemented by natural gas, varied distribution of renewable energy between wind and wave power, and varied power capacity of a compressed air energy storage system supplying power to a shoreline community. For each parameter set, we consider the historical hourly electricity demand and wind-sea data of a coastal California community over a year, and optimize the energy storage schedule to reduce curtailed power, stored energy, and base gas plant operational cost. We show that a co-located wind-wave farm has smoother power supply, less energy curtailment, and higher farm-to-grid efficiency than a solely wind farm. That is, a 50%–50% wind-wave farm has a 15% smaller coefficient of variation in the power supply, 6% less curtailed power, and 2% higher farm-grid efficiency than a 100% wind farm when the grid is 100% renewable energy. These benefits of wave power potentially decrease the need for interconnecting regional transmission lines to match power supply with demand. The intent of this paper is to provide baseline system technical results to help future researchers and policy makers make decisions about offshore hybrid wind-wave-storage farms.

1. Introduction

Increasing global energy demand and the push for lower global carbon emissions have increased the demand for renewable energy (RE) technologies. Since renewable energy tends to be highly variable from one hour to the next, grids with a high RE grid penetration face supply–demand matching operational challenges [1].

Typical methods for improving RE supply–demand matching include diversification of the RE resource type or location and adding energy storage systems. Previous studies have found that maximizing RE resource type diversity enables a more reliable, less variable, and more predictable RE supply [2–5]. The main challenge of diversifying the resource location is that it requires a large amount additional high-powered transmission lines to transfer power from areas of oversupply to typically urban areas with under-supply, which increases cost [5].

Previous studies have found that energy storage systems play vital roles in the load following, spinning reserve, peak shaving, time shifting, and unit commitment capabilities of renewable energy. In this paper, we consider long-term grid control, over time spans of multiple hours. The main challenges with long-term energy storage are determining how to lower the system capital cost, increase the energy capacity, improve power efficiency, and optimally manage the grid for overall electricity cost [6]. Numerous types of energy storage systems are viable for improving the hourly supply–demand balance of RE power. The most common long-term storage types are compressed air and pumped hydro [7].

In this paper, we investigate renewable energy cost and supply–demand matching challenges specifically for offshore wind and wave renewable energy. With higher, more consistent wind speeds, and less

[☆] The short version of the paper was presented at the Applied Energy Symposium: MIT A+B, August 11–13, 2021, Boston.

* Corresponding author.

E-mail address: jociek@alum.mit.edu (J.M. Kluger).

¹ Co-first authors.

visibility, offshore wind has the potential for cheaper, more manageable electricity than onshore wind. Floating wind turbines (FWTs) are considered more economically viable than fixed-bottom offshore wind turbines in ocean sites with depths beyond 60 m [8]. However, FWTs must be carefully designed to limit undesirable platform motions which increase stresses on the tower base, rotor shaft, yaw bearing, and blades [9], while also reducing aerodynamic efficiency and complicating rotor aerodynamics and control [10–12]. Platform stabilization is often solved using a large steel and/or concrete platform mass, active water ballast, or taut mooring lines [10,13,14]. This use of increased structure, as well as the needed offshore electric infrastructure, causes FWTs to be 2–3 times more expensive than onshore wind, with levelized costs of energy (LCOE) ranging from \$0.12–0.27/kWh, as compared to \$0.04–\$0.07/kWh for onshore wind [13,15,16]. While this paper focuses on a spar FWT platform, different FWT platforms have different trade-offs in capital cost and stability that affect the power and cost performance [15,17–20].

As a less mature industry than the wind industry, wave power is currently much more expensive. Wave farms have predicted energy costs ranging from \$0.35–0.85/kWh [21,22]. The wide range reflects the cost uncertainty. However, since wave power has less variation and higher predictability than wind, many studies have concluded that wave power has the potential help integrate renewables into the electric grid [1,4,23]. While this paper focuses on a heave point absorber WEC, different WECs have different power capacity factors that affect the power and cost performance [24–26].

In addition to smoothing power supply, previous studies have shown that co-locating wave energy converters (WECs) with wind turbines can have synergistic effects on the system costs [24,27–30]. Shared cost opportunities during project development include site characterization and permitting, stakeholder engagement, and infrastructure planning. Co-location permits cost sharing of the transmission lines. If the WEC is physically attached to the FWT, then sharing of mooring lines, steel frame, and electrical infrastructure has the potential to reduce the WEC cost by 50% [24,31,32]. During operation, the co-location also permits the sharing of maintenance logistics [33–35].

Significant research is required to optimize the coupled mechanical dynamics and hydrodynamics of a combined FWT-WEC [36–44]. Offshore farm layouts that place WECs and FWTs near each other permit the WECs to shield the FWTs from waves, thereby decreasing problematic FWT motion and increasing maintenance accessibility to the FWTs [41]. Preliminary studies on the dynamics of physically attached FWT-WECs have shown that the WEC can significantly reduce FWT surge and pitch motion [36,37,42]. Haji et al. [37] predicted that physically attaching a WEC to a FWT can reduce the FWT lifetime equivalent tower root stress by 23%. Although [36,37,42] found that the physical combination increased FWT heave motion, future work may investigate how adding a heave plate and adjusting FWT platform buoyancy may reduce any problematic heave motion. Similarly, further work may investigate optimizing the ratio of the WEC and FWT platform sizes and implementing a locking mechanism for survival during extreme waves [38]. Studies that have investigated the hydrodynamic interaction between the floating bodies of the FWT's and WEC's include [36,39,40,43,44].

This study focuses on technical issues associated with high penetration RE, while not considering a particular set of policy efforts. While it is beyond the scope of this paper, offshore RE policy should consider the impact on the local society and industry. Construction, operation, and management of the RE farm may provide jobs to the local community [45]. The farm may also generate tax revenue. Since the farm is sufficiently far from the shoreline, it should have negligible or positive impact on tourism [45,46]. Offshore energy production can have negative impacts on birds and marine mammals while having some positive benefits on fish [47].

In this paper, we investigate how incorporating wave power into an offshore wind farm affects farm power predictability, smoothness,

required energy storage capacity, and cost. Our approach is to consider the power and cost performance of an isolated electric grid supplied by varied capacities of wave power, wind power, conventional gas power, and energy storage for meeting the demand of a nearby shoreline community. Section 2 describes the power generation and power flow models with losses. Section 3 describes the cost of energy model. Section 4 describes the methodology of a parameter sweep that varies the renewable energy penetration level, fraction of RE from wind or wave, and power capacity of a compressed air energy storage system. Section 5 describes the energy storage schedule optimization method used to match supply and demand while minimizing renewable energy cost amid conventional power plant constraints. Section 5 describes the parameter sweep results. Section 6 discusses the results, and Section 7 makes final conclusions about the role of wave power in supply-demand matching.

2. Power modeling methodology

In this paper, we consider an electric grid power-flow scenario with fluctuating supply and demand and power losses in an isolated system. The value of studying an isolated grid scenario is that it presents bounds on the system performance when there is minimal interconnecting transmission lines. The power supply consists of the offshore wind and wave farm supplemented by a natural gas plant. The wind and wave supply and grid demand are based on hourly data recorded during 2017 near Eureka, California. Climate and electricity consumption changes since 2017 have likely not changed significantly enough to affect the first-order conclusions of this study. Future work can investigate the results' sensitivity to climate change. Compressed air energy storage (CAES) helps match the power supply to the grid power demand. The wind-wave-storage farm analyzed in this study is suitable for the target region indicated in Fig. 1 on the Northwest United States coast, which has onshore geology compatible with CAES and strong offshore wind and wave resources [48].

2.1. Wind energy resource

We base the wind turbine power on a steady-state power curve applied to real historical buoy data. The power curve is scaled up from a Siemens SWT-3.6 MW turbine to a 6 MW capacity as shown in Fig. 2 [49]. The wind turbine power model subtracts 5% array losses and 3.5% soiling losses from the ideal power curve [50].

Wind speed data is collected hourly throughout the year 2017 by the National Oceanic and Atmospheric Administration (NOAA) National Buoy Database Station 46 022, which is approximately 17 nautical miles south west of Eureka, California, as shown in Fig. 1. This paper assumes that all of the wind turbines experience the same wind speed at hub heights of 97 m. The buoy's near-sea-level wind speed measurement is scaled to wind speed at the hub height by,

$$v_r = v_a \left(\frac{z_r}{z_a} \right)^v, \quad (1)$$

where v_r is the wind speed at the hub height $z_r = 97$ m, v_a is the measured wind speed at the buoy height $z_a = 5$ m, and v is the power law wind speed shear exponent, set to 0.11 [51]. Based on the power curve with losses in Fig. 2 and the wind speed data from NOAA buoy 46 022, each wind turbine produces an average of 2.2 MW throughout 2017. This equates to a power capacity factor of 36%.

2.2. Wave energy resource

We base the wave energy converter power on the National Renewable Energy Laboratory RM3 WEC power matrix as shown in Fig. 3, which predicts the wave energy converter electric power as a function of significant wave height and peak wave period, assuming a Bretschneider sea spectrum [21]. In this first-order study, we do

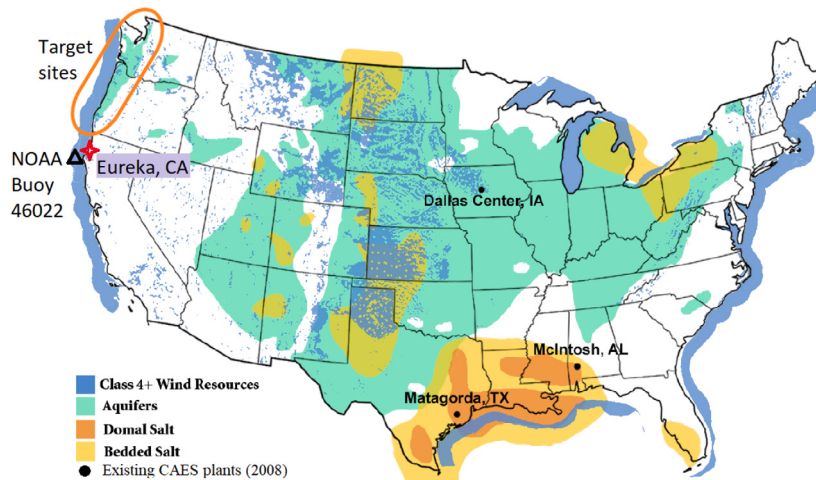


Fig. 1. Map of offshore wind resource and onshore geology compatible with compressed air energy storage. In this study, the hourly wind and wave data is obtained from National Oceanic and Atmospheric Administration buoy 46022, and the hourly electricity demand data is obtained for an electric grid node near Eureka, California. This data has similar characteristics to the west coast of Oregon and Washington, which have suitable geology for installing a compressed air energy storage system.
Source: Figure adapted from Succar and Williams [48].

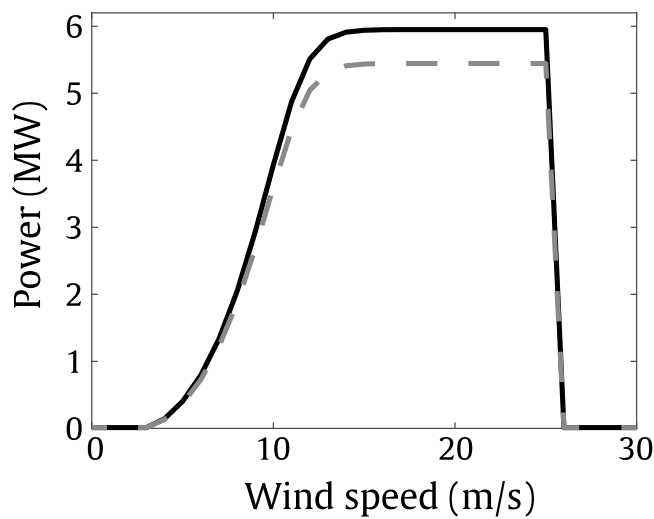


Fig. 2. Wind turbine power curve scaled from a Siemens SWT-3.6 MW turbine for a 6 MW capacity. Ideal (solid) and with 8.5% soiling and array losses (dashed) [50].

not distinguish different WEC power productions for the standalone WEC's and combined FWT-WEC's. This paper estimates the wave energy converter power using the hourly significant wave heights and peak wave periods recorded by NOAA buoy 46 022 during 2017, which is the same time period and buoy used for the wind energy resource. Fig. 1 indicates the buoy location 17 nautical miles WSW of Eureka, California. Based on the WEC power curve and buoy data, each WEC produces an average of 69 kW throughout 2017. This equates to a power capacity factor of 24%.

2.3. Compressed air energy storage

The compressed air energy storage system stores energy as compressed air in an underground storage cavern. Since the self-discharge of the system is very low, CAES systems are considered long-term time scale storage installations which can compete with pumped hydro storage. When the electric grid requires an energy injection, the compressed air is drawn from the storage cavern, heated, and then expanded through a set of high and low pressure turbines which convert most of the compressed air energy into rotational kinetic energy. The air is

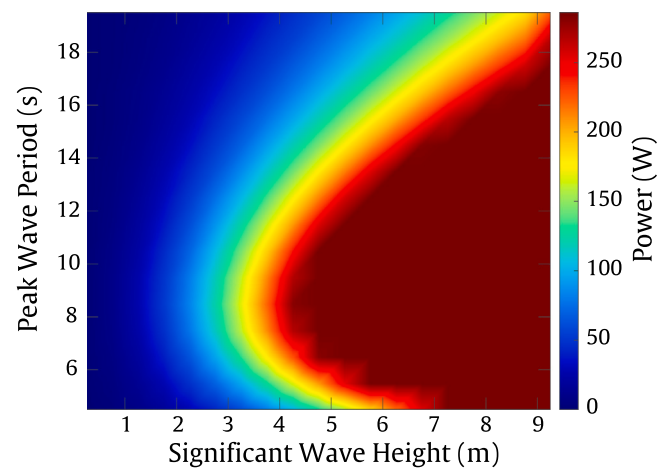


Fig. 3. NREL RM3 Wave energy converter electric power curve.
Source: Adopted from Neary et al. [21].

additionally mixed with natural gas and combusted. While the turbines are connected to electrical generators in order to obtain electrical energy, the turbine exhaust is recirculated to heat the cavern air [7]. A schematic of the CAES system is shown in Fig. 4.

Compressed air energy storage can use a variety of storage vessels, such as salt caverns, hard rock caverns, porous rock formations, abandoned mines, pipes, underwater bladders, and above-ground tanks. This paper assumes porous/aqueous rock is used, due to its low cost, as shown in Table 2, and presence on the northwest coast of the Unites States, as shown in Fig. 1. A variety of fuels, such as hydrogen, natural gas, gasified biomass, and oil can be used in the combustion process [52]. This paper accounts for fuel in the CAES operational cost of \$2.52/MWh energy flow into the storage system, as described in Section 3 and Table 4. In general, power efficiency estimates for traditional large CAES systems fall between 73% and 89% [52–54]. This paper assumes a power efficiency of 90% when power enters and leaves the storage system (81% round-trip efficiency). Pressure limitations affect how deeply a CAES system can charge or discharge [55] and therefore may cause the energy storage system to be sized larger than if it did not have these limitations. As described in Section 3, the cost of energy storage systems is dominated by the power component (\$1.43 million/MW) rather than the storage component (\$100/MWh).

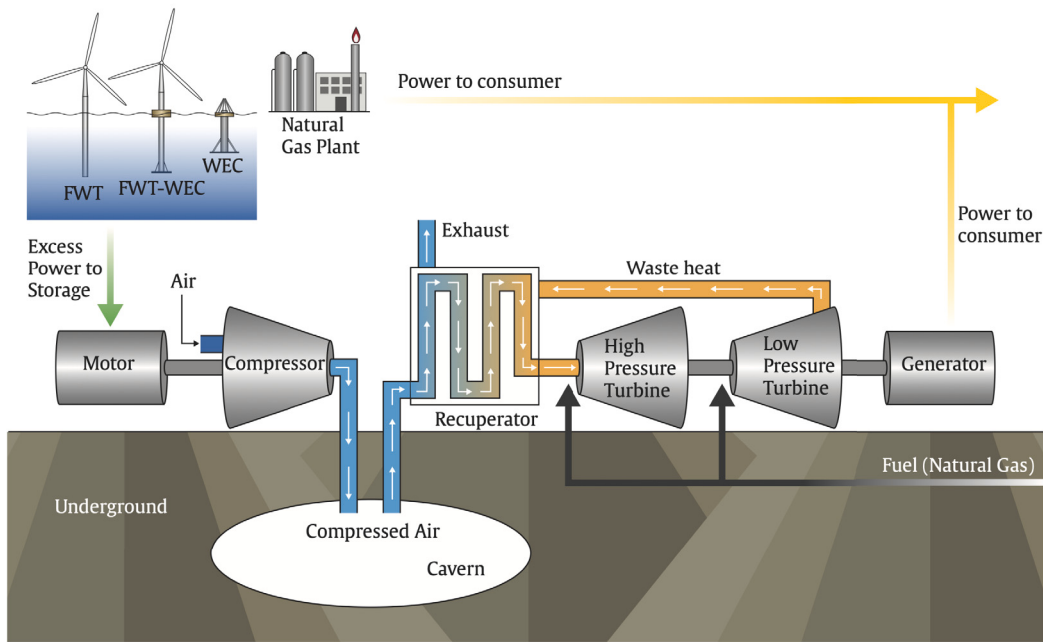


Fig. 4. Compressed air energy storage system (CAES) system schematic. Excess power from the offshore renewable energy farm and natural gas power plant is used to compress air. The air is pumped underground and stored for later use. When electricity is needed, the compressed air is used to run a gas-fired turbine-generator. The electricity produced is delivered back to the grid.

Source: Adapted from Díaz-González et al. [7].

2.4. Natural gas power plant

In this study, an open-cycle natural gas turbine power plant provides a base power supply to the electric grid. The plant is sized so that its capacity equals the peak demand. One of the challenges of increasing renewable energy penetration is that it requires increasing power fluctuations from conventional power plants. The gas plant cycling flexibility and costs depend on the unit type, age, and usage pattern [56]. Typical conventional power plants have a minimum operational power output that ranges from 20%–40% of the plant capacity. Additionally, power plants have added costs and inefficiencies while ramping the power up and down, ranging from \$0.62–1.14/MW. This paper assumes that the power plant can operate at a minimum power output of 20% and power ramping costs \$1.05/MW.

2.5. Power demand

Fluctuating power demand is based on historical data from the California Independent System Operator (CAISO) database for the Eureka, CA grid node, which was collected hourly throughout the year 2017. Using real demand data at this location allows the model to represent realistic daily and seasonal power fluctuations that correlate with the wind and wave data from the nearby buoy.

Eureka, California is a small city of about 25,000 residents in Humboldt County, a rural region on the northern coast of California. Following [57], electricity use in Humboldt County is divided among residential (approximately 45%), commercial (approximately 38%), and industrial sectors (approximately 16%). The climate is temperate, with cool summers and mild winters, which reduce the heating and cooling needs relative to other regions in the United States. The majority of electricity consumption in the residential and commercial sectors is for lighting and refrigeration. Natural gas is used for most water heating and space heating in the residential and commercial sectors [57].

In this paper, we scale the demand so that the mean annual power demand multiplied by the renewable energy penetration fraction matches the mean renewable energy power supply. The analysis in this

paper does not consider the natural gas usage for heating. Accounting for that natural gas demand would decrease predicted gas plant relative ramping requirements and could be part of a future study.

2.6. Electrical transmission

The power flow model accounts for losses in the offshore and onshore converter stations and submarine cables. For the offshore wind-wave farm considered in this study, the electric transmission losses are on the order of 2.7% of the electricity generated by the wind and wave power machines.

The electrical transmission system consists of a medium voltage alternating current (MVAC) 34.5 kV submarine array that collects the power produced by the FWTs and WECs and delivers it to the offshore high voltage alternating current (HVAC) substation. The HVAC substation steps voltage up to the export voltage and transmits it through the 220 kV HVAC submarine cables to the onshore converter station. The onshore converter station steps voltage up to 500 kV for integration with the U.S. grid. Following Todorovic [58], the power losses at both converter stations are modeled according to,

$$P_{Loss,Transformer} = 3 \frac{U_{Nom}^2}{R_{Fe}} + I^2 R_{Cu}, \quad (2)$$

where U_{Nom} is the nominal voltage in the cables, R_{Fe} is the transformer equivalent resistance from iron losses, R_{Cu} is the transformer copper resistance, and I is the fluctuating input current to the converter station.

In the case study of this paper, the transmission distance from the offshore site to shore is 50 km. Previous work has suggested that for transmission over distances of 55 km or less, HVAC transmission is the most economical [59], with 80 km considered the crossover distance between HVAC and high voltage direct current (HVDC) [60]. Hence, the offshore energy farm modeled in this paper uses a submarine HVAC transmission cable that consists of three 220 kV, 300 MW-rated, 50 km long cross linked polyethylene cable (XLPE) cables, using a power loss model described in Todorovic [58] and cost model described in Beitner et al. [61]. The model described by [58,62,63] accounts for HVAC cable

Table 1
Offshore farm plant financing assumptions, taken from [61].

Variable	Value
Project lifetime	20 years
Inflation rate	2.5%
Combined State and Federal Tax Rate	40%
Construction Finance Rate	8%
Construction on time	2 years
Internal Rate of Return	10%
Debt Fraction	50%
Return on Debt	8%
After Tax Weighted Average Cost of Capital	7.4%
Modified Accelerated Cost-Recovery System	5 years
Calculated Fixed Charge Rate	10.51%

power losses as a function of cable current and temperature. These losses are due to reactive currents, cable length, and compensation. We assume that the conductors are 90 °C and the ambient temperature is 15 °C.

3. Cost modeling methodology

The levelized cost of energy (\$/MWh) of the overall offshore wind-wave farm is determined by,

$$\text{LCOE} = \frac{\text{ICC} \times \text{FCR} + \text{AOE}}{\text{AEP}}, \quad (3)$$

where ICC (\$/MW) is the total installed capital cost, FCR is the fixed charge rate, AOE (\$/MW-yr) is the annual operating cost, and AEP is the annual energy production.

FCR takes into account the cost of financing, taxes, and depreciation. This study uses an FCR value of 10.15% following Beiter et al. [61]. Additional financing assumptions are detailed in Table 1 and also pulled from Beiter et al. [61]. The inflation rate is taken to be 2.5% based on historical data at the time of publishing Beiter et al. [61]. We note that the inflation rate in 2022 is different from that in 2016. However, because the inflation rate has a cascading effect on a number of other computed financial parameters (such as FCR), modifying the inflation rate and corresponding financial parameters is out of the scope of this study. In this study, the relative performances of different parameter sets are relatively insensitive to the FCR.

ICC is the sum of all the capital costs of the farm, which include all standalone FWTs, standalone WECs, combined FWT-WECs, the energy storage system, and the electric infrastructure. AOE takes into account all necessarily maintenance and operation for these components. In this paper, the constant AOE throughout a system lifetime accounts for changing operating costs over time including categories such as installation, commissioning, operations, maintenance, and decommissioning. All FWT capital and operational costs are taken from Beiter et al. [61], and all WEC costs are taken from Neary et al. [21]. This paper adjusts these costs to 2022\$.

The offshore farm capital and operating costs decrease significantly as the number of installed units increases from a single to many units. Fig. 5 illustrates this trend in the ICC and AOE for the WECs considered in this study.

As described in [24], the FWT-WEC share a number of common elements, which decreases the capital and operating costs per MW of the combined device compared to a standalone WEC. The FWT spar buoy serves as the reaction body for the point-absorber WEC. The central spar structure is augmented by a 245 metric ton steel reaction plate at the platform keel to resist heave motion. The spar concrete platform ballast is decreased by 245 metric tons to maintain buoyancy after adding the reaction plate. The FWT and WEC share the electrical infrastructure and mooring system.

Fig. 5 compares the capital and operating costs of a standalone WEC, WEC portion of a combined FWT-WEC, and total combined FWT-WEC. Fig. 5 shows a cost reduction for the WEC component of a combined

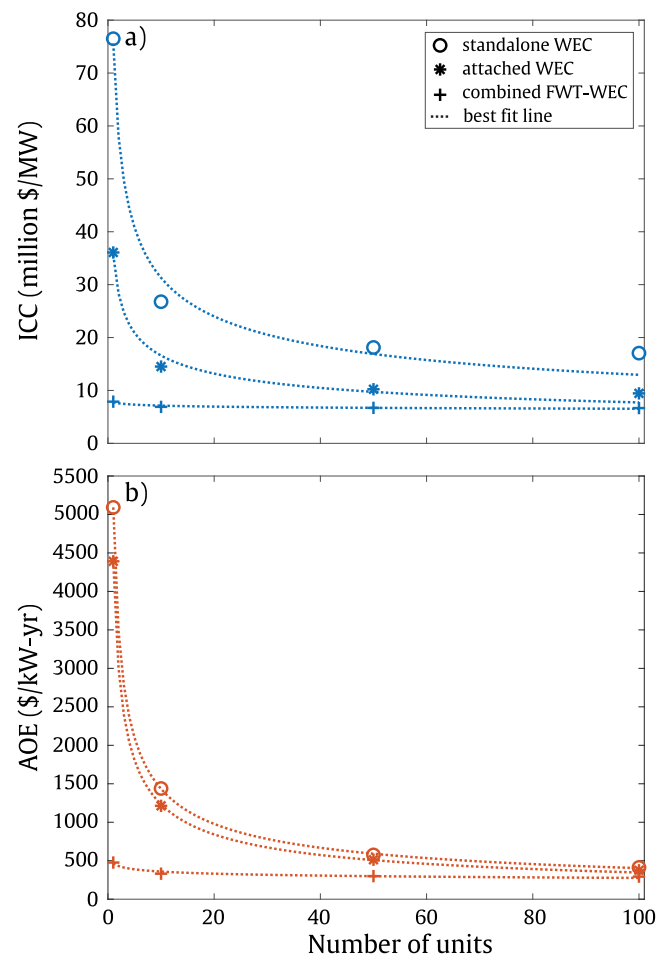


Fig. 5. (a) ICC (\$/kW) and (b) AOE (\$/kW-yr) of standalone WEC (○), WEC that is attached to a FWT (*), and total combined FWT-WEC (+), from Neary et al. [21,61], adjusted for 2022 \$. Dashed lines indicate the exponential best fit for each device type. The ICC and AOE of the standalone FWT is held fixed to \$6.4 million/MW and \$289/kW-yr, respectively [61].

FWT-WEC compared to a standalone WEC. For the parameter sweep procedure in this study, the ICC and AOE are taken as constant values corresponding to 100 units for both the standalone and attached WECs. The ICC and AOE of the standalone WECs are held fixed to \$17.0 million/MW and \$412/kW-yr, respectively. The ICC and AOE of the standalone FWTs are held fixed to \$6.4 million/MW and \$289/kW-yr, respectively [61]. The ICC and AOE of the combined FWT-WECs are taken as \$9.43 million/MW and \$374/kW-yr, respectively.

AEP is the sum of the annual energy produced by each energy source in the farm. Each 6 MW wind turbine produces an average power of 2.2 MW and each 286-kW wave energy converter produces an average power of 69 kW throughout the year, as described in Section 2.1 and 2.2, respectively.

The LCOE also accounts for the cost of the energy storage system. While some compressed air energy storage system (CAES) installations may last up to 40 years [64], we model the lifetime as 20 years to align with the lifetime of the rest of the farm. The capital cost for the energy storage system tends to be dominated by the motor, compressor, and turbine-generators. We use a cost of \$1.43 million/MW for these power components, based on Zakeri and Syri [65]. Additionally, the capital cost has a smaller component that scales with stored energy capacity. Table 2 describes the estimated capital costs per energy capacity of CAES systems for different geological formations and mining techniques. In this paper, we use a storage cost of \$0.10/kWh, representing

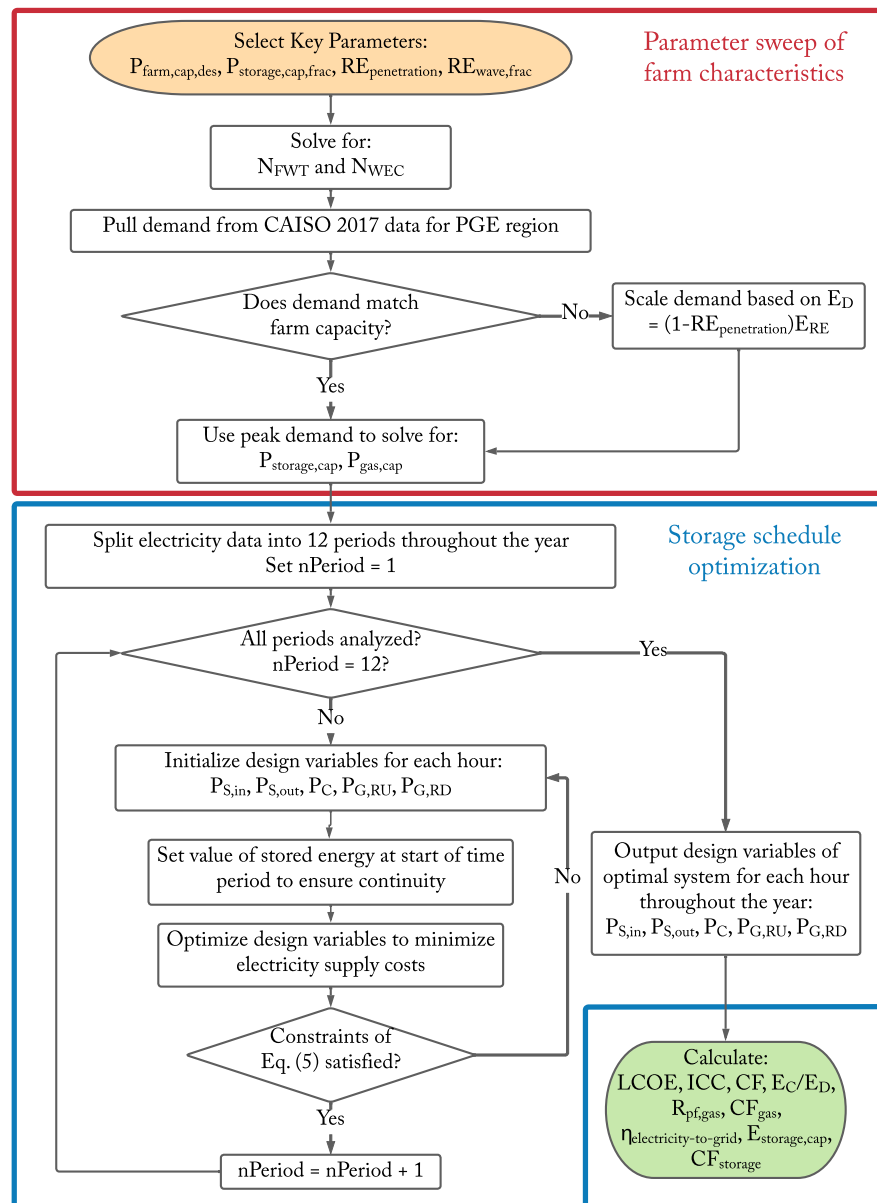


Fig. 6. Flow chart showing the parameter sweep (Section 4) and optimization process (Section 5) conducted in this study.

Table 2

Capital costs of bulk CAES storage by geology [52] (costs presented below in 2009 \$ and later adjusted to 2022 \$ for analysis in this paper).

Geology	Capital costs
Salt Cavern (solution mined)	\$ 1/kWh
Salt Cavern (dry mined)	\$ 10/kWh
Hard Rock (excavated and existing mines)	\$ 30/kWh
Porous Rock/Aquifer	\$ 0.10/kWh
Abandoned Limestone or Coal Mines	\$ 10/kWh

an aquifer. During operation, we assume a cost of \$2.52/MWh as energy flows into and out of the CAES, which follows results by Liu et al. [66] and Zakeri and Syri [65].

This study does not explicitly include the gas plant costs in the LCOE calculation since the focus is on minimizing the renewable energy costs. As described in Section 5 and Table 4, the optimization objective function includes the cost of gas plant start-up and ramping. Future studies could more extensively study the natural gas power plant costs

during a gas plant phase-out and transition to a 100% renewable electric grid.

4. Parameter sweep methodology

We use parameter sweeps to compare the power statistics and cost of renewable energy systems with different characteristics. For renewable energy penetration levels of 50%, 75%, and 100%, parameter sweeps vary the compressed air energy storage (CAES) power capacity and the fraction of renewable energy from ocean waves. The remaining renewable energy is from wind. This study represents a scenario of minimal interconnecting transmission lines with the rest of the electric grid. Interconnecting transmission lines introduce power smoothing but at additional cost [5]. Fig. 6 summarizes the steps in the parameter sweep and how it incorporates the energy storage schedule optimization described in Section 5.

The renewable energy supply power capacity ($P_{farm,Cap}$) is held fixed to 600 MW. The number of WECs and FWTs are adjusted to fit the 600 MW farm capacity and fraction of renewable energy from ocean

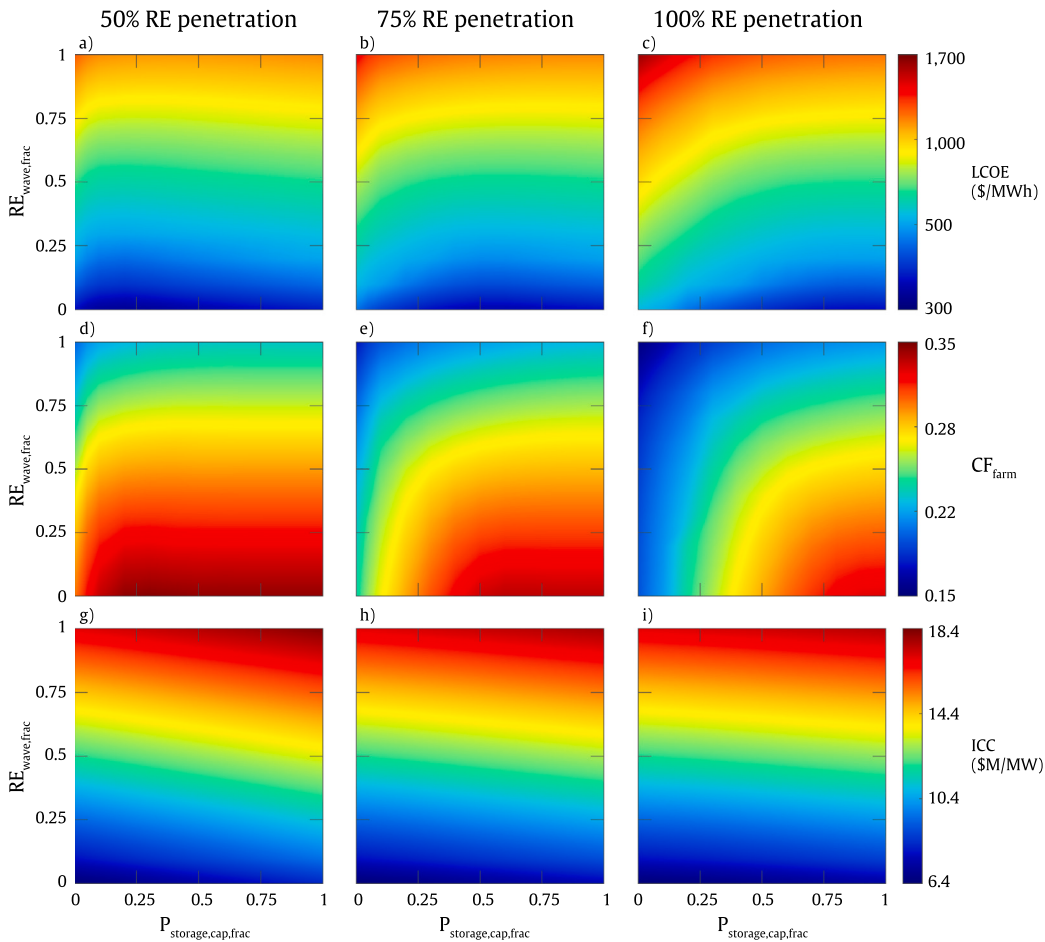


Fig. 7. Optimized leveledized cost of energy ($LCOE$, row 1), capacity factor (CF_{Farm} , row 2), and installed capital cost (ICC , row 3) for varied renewable energy penetration levels (columns 1–3). The color bar to the right of each row defines the color scale for all plots in the row. CF_{Farm} accounts for transmission losses, storage losses, power curtailment, and the environmental wind and wave fluctuations that prevent the farm from constantly producing 600 MW. The horizontal axis varies the energy storage power capacity as a fraction of the peak community demand ($P_{storage, cap, frac}$), and the vertical axis varies the fraction of renewable energy from wave power ($RE_{wave, frac}$).

waves ($RE_{frac, Wave}$). That is, when the offshore farm is 100% wind, the farm contains 100 6-MW wind turbines. When the farm is 100% wave, the farm contains 2098 286-kW wave energy converters. For farms that contain a mix of wind and wave power, one wave energy converter is attached to each wind turbine while any remaining wind turbines or wave energy converters are standalone structures. Since many standalone WECs are required to reach comparable power to a single FWT, the combined FWT-WEC systems have a relatively low impact on the total farm cost.

The community's electricity demand is scaled to represent the chosen RE penetration level according to:

$$E_D = \frac{E_{RE}}{RE_{Penetration}}. \quad (4)$$

where E_D is the annual energy demand, the sum of the hourly power demand over the entire year, as described in Section 2.5. $RE_{Penetration}$ is the renewable energy penetration level, and E_{RE} is the annual energy transmitted by the wind-wave farm after all losses except storage losses.

We set the gas plant power capacity ($P_{Gas, Cap}$) to match the annual peak power demand. This represents a scenario of increasing renewable energy penetration to a grid that is originally fully supplied by a conventional power plant. The gas plant minimum stable power output is 20% of its full capacity, which represents a flexible combined cycle gas turbine [67].

The compressed air energy storage system power capacity is varied as a fraction of the annual peak power demand and referred to as $P_{storage, cap, frac}$. The energy storage capacity is a result of the energy storage schedule optimization described in Section 5.

At each parameter sweep point, after the design variables are optimized for the entire year, as described in Section 5, the following farm performance quantities are calculated: leveled cost of energy ($LCOE$), capacity factor (CF_{Farm}), installed capital cost (ICC), ratio of energy curtailed to renewable electricity produced (E_C/E_{RE}), ratio of gas plant power fluctuation to mean power ($R_{pr, gas}$), capacity factor of the gas plant (CF_{gas}), electricity-to-grid efficiency ($\eta_{electricity-to-grid}$), energy storage capacity ($E_{storage, cap}$), and the capacity factor of the storage system ($CF_{storage}$).

5. Energy storage schedule optimization methodology

For each RE system parameter set, we use linear optimization to adjust the energy storage schedule and capacity to minimize operational cost while matching power supply with demand and satisfying the gas plant operational constraints. The optimization procedure is described below and outlined in the bottom half of Fig. 6.

We implement a primal-simplex mixed integer linear optimization algorithm in MATLAB to optimize design variables related to storage system power flow, gas plant power, and curtailed power. The optimization problem assumes that the farm operator has access to perfect supply and demand forecasting data over an entire year. While the optimization is solved with an hourly resolution over an entire year, the problem is divided into 12 periods to speed-up the optimization computation. To ensure continuity, the value of energy stored at the end of the previous period is used as the initial energy stored at the beginning of the next period.

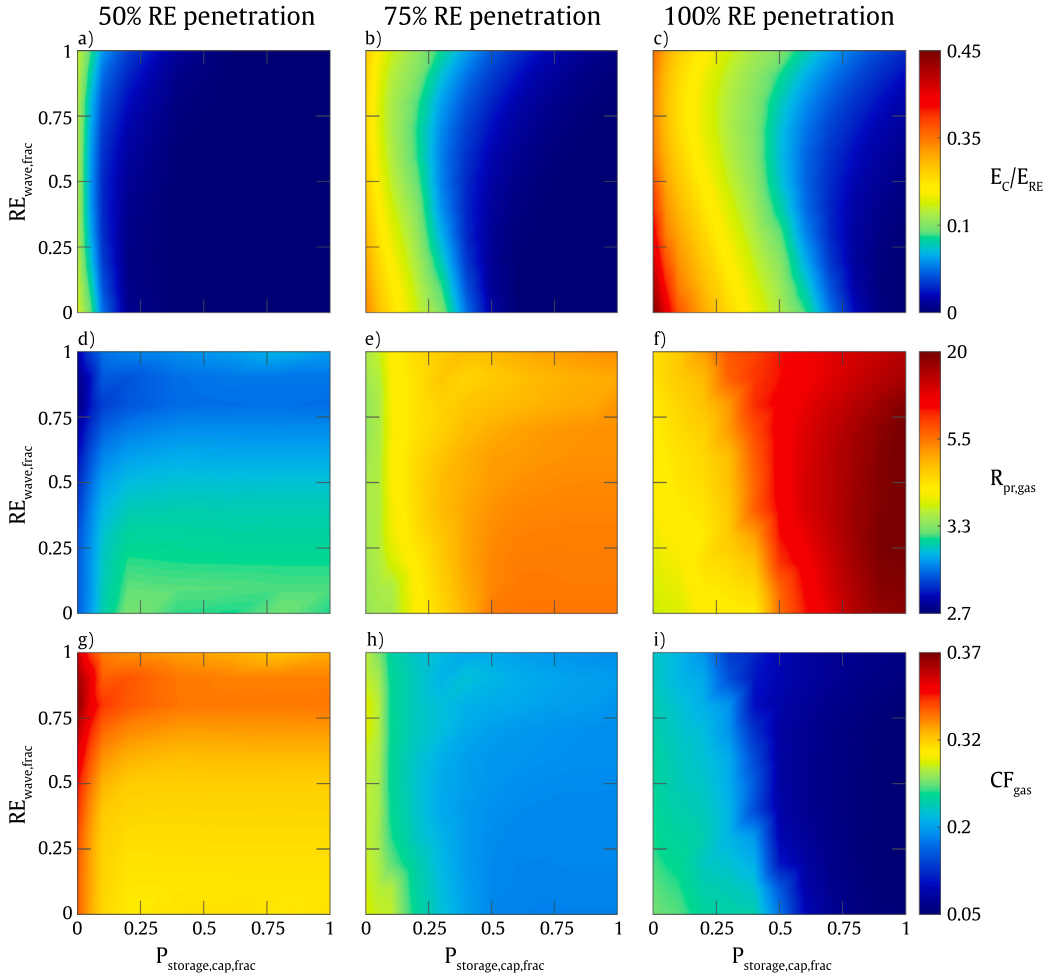


Fig. 8. Optimized fraction of curtailed energy (E_C/E_{RE} , row 1), gas plant ratio of power fluctuation ($R_{pr,gas}$, row 2), and farm capacity factor (CF_{gas} , row3) for varied renewable energy penetration levels (columns 1–3). The color bar to the right of each row defines the color scale for all plots in the row. The horizontal axis varies the energy storage power capacity as a fraction of the peak community demand ($P_{storage,cap,frac}$), and the vertical axis varies the fraction of renewable energy from wave power ($RE_{wave,frac}$).

The optimization algorithm minimizes the objective function subject to the constraints in Eqs. (5a)–(5i).

$$\text{minimize} \quad \sum_h Cost_S P_{S,in} + Cost_C P_C + Cost_G \quad (5a)$$

$$\text{where} \quad Cost_G = Cost_{G,R} (P_{G,RU} + P_{G,RD}) + Cost_{G,Si} G_{TO}, \quad (5b)$$

$$\text{subject to} \quad P_{FWT} + P_{WEC} - P_{S,in} + P_{S,out} + P_G - P_C = P_D, \quad (5c)$$

$$E_{S,h-1} + \eta_S P_{S,in,h} - \frac{P_{S,out,h}}{\eta_S} = E_{S,h}, \quad (5d)$$

$$\eta_S P_{S,out,h} \leq E_{S,h} \quad (5e)$$

$$G_{On,h} (1 - G_{On,h-1}) - G_{TO} \leq 0, \quad (5f)$$

$$0.2 G_{On} P_{G,Cap} \leq P_G \leq G_{On} P_{G,Cap}, \quad (5g)$$

$$G_{On}, G_{TO} \in \{0, 1\}. \quad (5h)$$

$$P_{S,in}, P_{S,out}, P_C, P_G, P_{G,RU}, P_{G,RD} \geq 0, \quad (5i)$$

Table 3 lists the design variables. **Table 4** lists the fixed parameters and prescribed hourly power conditions in the optimization problem.

The annual system operational cost in the objective function, Eq. (5a) is the sum over all hours (h) of three costs: the energy storage cost, which is represented by a constant cost per MW ($Cost_S$) multiplied by the power entering the storage system ($P_{S,in}$); the curtailed power cost, which is represented by a constant cost per MW ($Cost_C$) multiplied by the power curtailed (P_C); and the operational cost of the gas plant,

Table 3
Legend of design variables in the optimization problem Eq. (5a)–(5i).

Name	Description
E_S	Stored energy
G_{On}	Integer flag that indicates the gas plant is on
G_{TO}	Integer flag that indicates the gas plant turns on
P_C	Curtailed power
P_G	Gas plant power
$P_{G,RD}$	Gas plant power ramp-down
$P_{G,RU}$	Gas plant power ramp-up
$P_{S,in}$	Power flow into storage
$P_{S,out}$	Power flow out of storage

which is represented by $Cost_G$ defined in Eq. (5b). This objective function implicitly contains the cost of energy inefficiency when power flows through the storage system since the lost power is ultimately replaced by gas power.

The operational cost of the gas plant, as defined in Eq. (5b), is comprised of two main components. The first component is the gas plant power ramping cost, which is represented by the ramping cost per MW ($Cost_{G,R}$) multiplied by the sum of the power ramp-up ($P_{G,RU}$) and ramp-down ($P_{G,RD}$). The optimization problem constrains $P_{G,RU}$ and $P_{G,RD}$ to always be greater than or equal to 0, and the optimization solution only ever has one of them greater than 0 at each hour. The cost to ramp the gas plant power up or down is set to $Cost_{G,R} = \$1.05/\text{MW}$, based on Van den Bergh and Delarue [56] and adjusted to 2022 \$.

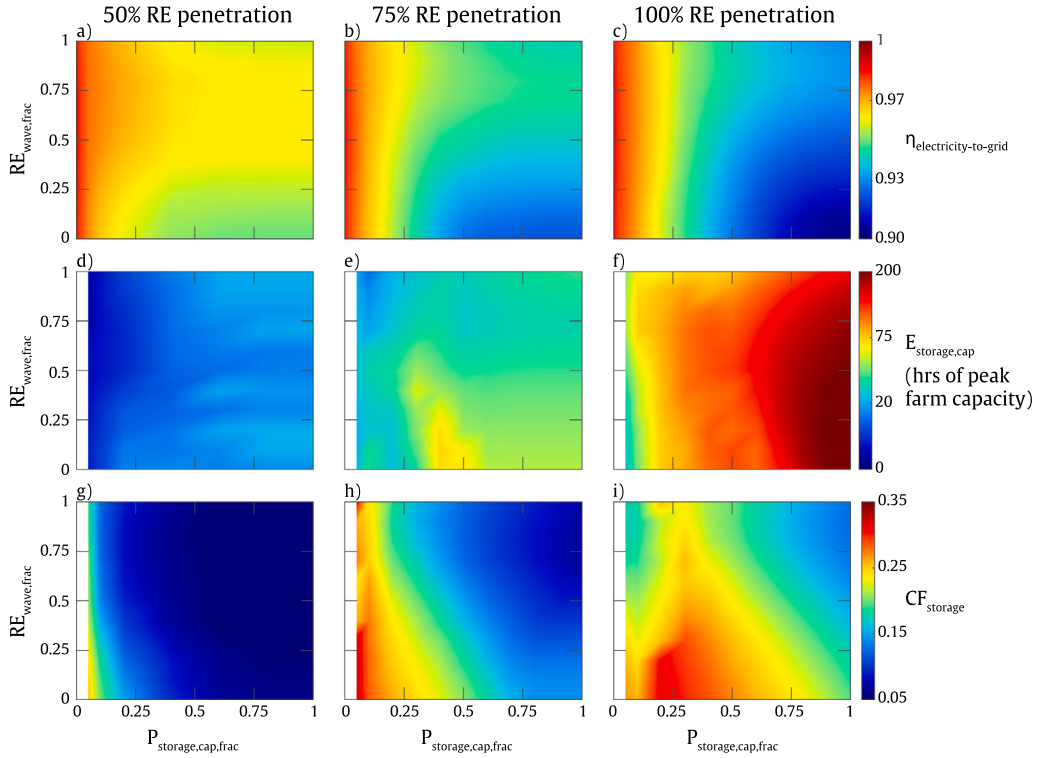


Fig. 9. Optimized efficiency ($\eta_{electricity-to-grid}$, row 1) due to transmission and storage losses, storage energy capacity ($E_{storage,cap}$, row 2), and storage power capacity factor ($CF_{storage}$, row 3) for varied renewable energy penetration levels (columns 1–3). The color bar to the right of each row defines the color scale for all plots in the row. The horizontal axis varies the energy storage power capacity as a fraction of the peak community demand ($P_{storage,cap,frac}$), and the vertical axis varies the fraction of renewable energy from wave power ($RE_{wave,frac}$).

Table 4
Parameters and prescribed power conditions in the optimization problem Eq. (5a)–(5i). All costs adjusted from references to 2022 \$.

Name	Description	Value	Reference
$Cost_S$	Cost of storage	\$ 2.52/MWh	[65,66]
$Cost_C$	Cost of curtailing power	\$13,133.30/MW	[56]
$Cost_{G,R}$	Cost to ramp the gas plant	\$1.05/MW	[56]
$Cost_{G,Si}$	Cost to start the gas plant	\$55.80/MW	[56]
η_S	Storage power efficiency	90%	[52–54]
$P_{G,min}$	Gas plant minimum operational power	$0.2P_{G,Cap}$	[56]
$P_{G,Cap}$	Gas plant power capacity	Peak demand	Section 2.4
P_{FWT}	Wind power	Varied	Section 2.1
P_{WEC}	Wave power	Varied	Section 2.2
P_D	Demanded power	Varied	Section 2.5
h	Hourly index of available sea state data	1 - 8740	NOAA Buoy 46022

The second component of the gas plant operational cost is the cost to start-up the gas plant ($Cost_{G,Si}$). This cost is incurred whenever the gas plant is turned on after being turned off. Eq. (5f), combined with Eqs. (5h) and (5i) constrains the gas plant turn-on flag (G_{TO}) to be 1 at the hour the plant turns on, and 0 otherwise. In Eq. (5f), h indicates the hourly time step. The cost to start the gas plant is set to $Cost_{G,Si} = \$55.80P_{G,min}$, based on Van den Bergh and Delarue [56] and adjusted to 2022 \$. $P_{G,min}$ is the minimum power that may be provided by the gas plant when it is operating ($G_{On} = 1$), and it is set to 20% of the gas plant power capacity ($P_{G,Cap}$) [56]. The gas plant power capacity ($P_{G,Cap}$) is set to the maximum of the power demand, P_D , for this study.

Eq. (5d) represents the accumulated energy in the compressed air energy storage system by tracking the inflow power ($P_{S,in}$) and outflow power ($P_{S,out}$) at each time step, h . The one-way power efficiency of the storage system, η_S , accounts for power losses during both power inflow and outflow of the storage system. The storage efficiency is set to $\eta_S = 90\%$ in this study. Eq. (5e) implements the constraint that the net flow of power out of the storage system cannot exceed the stored

energy. The energy storage capacity is not predetermined before the optimization, but is calculated as the maximum value of energy storage, E_S , during the entire year. The objective function Eq. (5a) implicitly minimizes the energy storage capacity and energy storage power losses through the $Cost_S P_{S,in}$ term.

Eq. (5c) is the grid supply-demand power balance. That is, the power demand (P_D) must be met by the net power provided by the renewable energy farm ($P_{FWT} + P_{WEC} - P_{S,in} + P_{S,out}$) and the gas plant (P_G), minus any power losses due to curtailment (P_C). Curtailment occurs when the renewable energy provides more power than the demand and than the storage system power capacity can absorb. That is, when so much power is produced that it cannot be adsorbed by either demand or energy storage. Curtailing power incurs a cost ($Cost_C$) in the objective function (5a), which is taken from Van den Bergh and Delarue [56] to be $Cost_C = \$13,133.30/\text{MWh}$ (in 2022 \$). The curtailment cost is an extremely large value to penalize energy curtailment during the optimization. $Cost_C$ is not directly used in the LCOE calculation in Section 4, where instead energy curtailment cost is accounted for through a decreased annual energy production for a

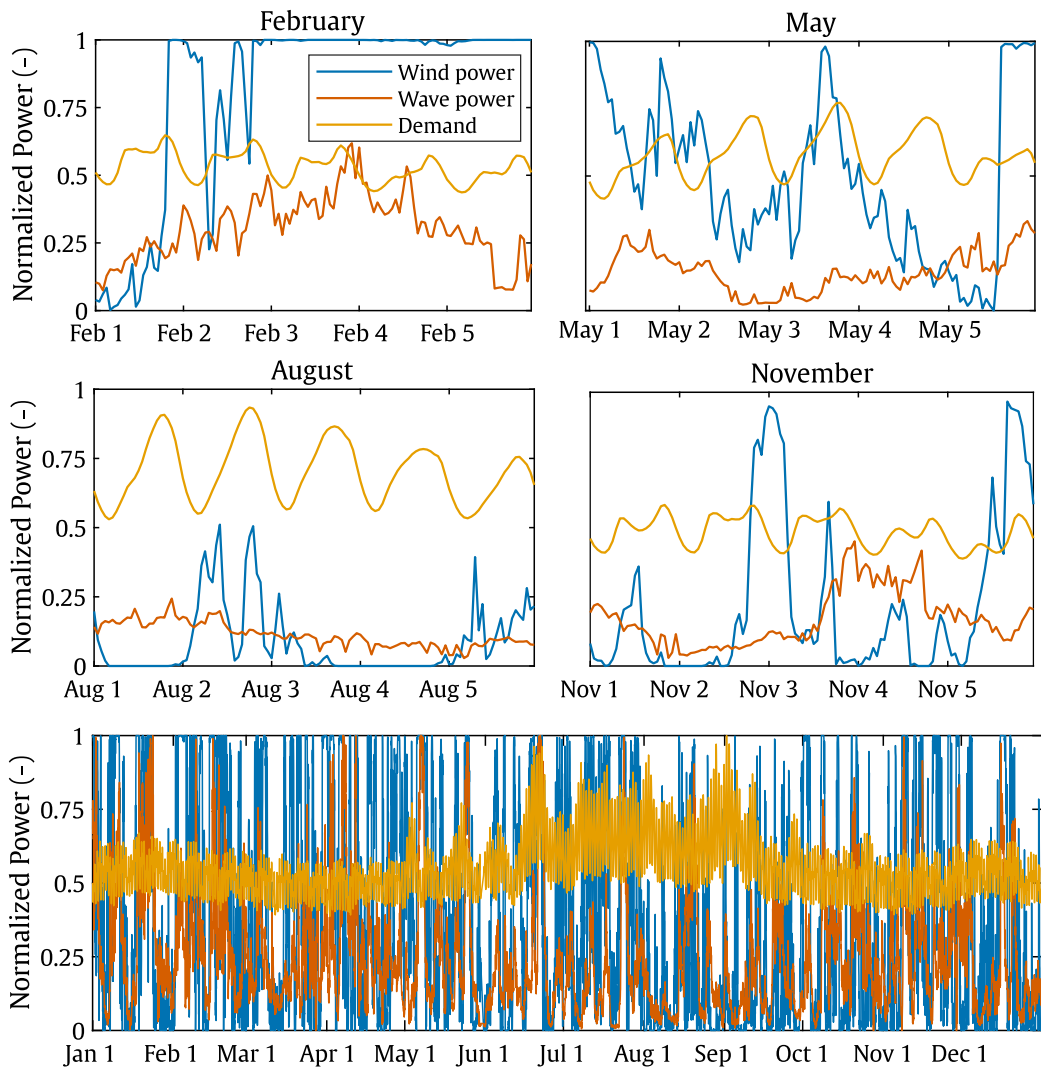


Fig. A.10. Seasonal and annual normalized wind power, wave power, and demand.

given capital cost. In particular, instead of curtailing power, the system is set to produce less energy so that there is no excess power that would not be able to be absorbed by demand and the energy storage system.

Based on the relative cost parameters, the objective function in this study gives the highest priority to avoiding energy curtailment, high priority to not turning the gas plant on and off, and the next priority to reducing energy flow through the storage system. This prioritization promotes gas plant power ramping, the least expensive source of controllable energy supply fluctuation. Additionally, the storage strategy does not give any penalty for the energy capacity of the storage system, which provides an idealized upper-bound size for an energy storage tank for supply–demand matching. Other studies have investigated storage control strategies that minimize energy curtailment by adjusting the storage schedule based on day-ahead forecasting, minimize the electricity flowing through storage to reduce storage inefficiency losses, or try to make the combined RE and storage output as constant as possible [68,69]. More realistic operation might also account for how the storage operator is driven by fluctuating electricity prices [68]. Finally, the most robust and optimized storage strategy may result from leveraging the large amount of historical demand and environmental data to develop artificial intelligence techniques such as long short-term memory (LSTM) networks [70]. Future work will investigate the effects of adjusting the energy storage control strategy.

6. Results

The results for renewable energy penetration levels of 50%, 75%, and 100% are shown in Figs. 7, 8, and 9, respectively. In each plot, the horizontal axis varies the energy storage power capacity as a fraction of the peak community demand, and the vertical axis varies the fraction of renewable energy from wave power. The remaining fraction of renewable energy is from wind power. We observe several trends across the varied renewable energy penetration levels, wave power fractions, and storage power capacities. Figs. B.12–B.15 in Appendix B show time series for systems with key parameter values that support these observations discussed below.

The least expensive LCOE occurs for 100% wind power. Increasing the fraction of wave power while holding the storage power capacity constant always increases the LCOE. This result is expected because the capital cost of wave power is far above that of wind power, and the overall farm installed capital cost significantly increases as the fraction of wave power increases. Beyond a moderate storage power capacity, increasing the storage power capacity does not affect the LCOE: avoiding energy curtailment (shown in Fig. 8) is balanced with adding capital cost to the storage system. For increasing RE penetration, this crossover point occurs at larger storage power capacities. The capital cost is relatively insensitive to the storage power and energy capacity compared to wave power. The LCOE is relatively insensitive

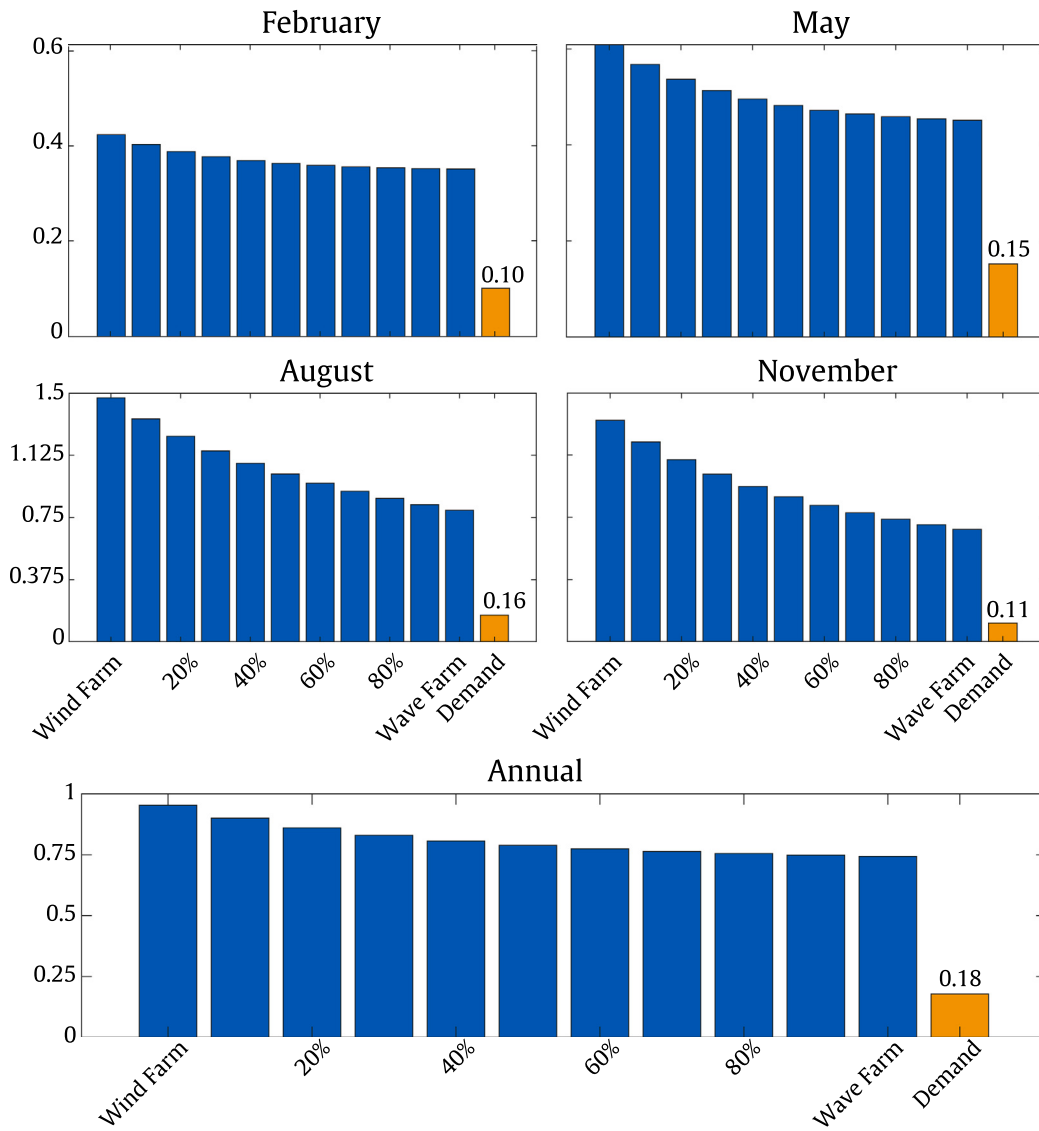


Fig. A.11. Seasonal and annual coefficient of variation of offshore farm power with different power capacity distributions between wind and wave. The seasonal subplots are based on the same 5-day periods as shown in Fig. A.10.

to the RE penetration when there is moderate or high storage power capacity.

For all RE penetration levels, the curtailed energy increases significantly when the storage power capacity is below a certain threshold. This storage power capacity threshold increases from about 10% to 50% of peak demand when the RE penetration increases from 50%, to 100%. For a fixed storage power capacity, mixing wind and wave power decreases power curtailment compared to a pure wind or pure wave supply. When RE penetration is 100% and storage power capacity equals 50% of peak demand, wave power decreases curtailed power by 3%–6%. That is, a 100% wind farm, 50%–50% wind-wave farm, and 100% wave farm have 13%, 7%, and 10% of the renewable energy curtailed, respectively.

The farm efficiency, $\eta_{\text{electricity-to-grid}}$, shown in Fig. 9, accounts for transmission losses and energy storage losses (not curtailed energy). The electricity-to-grid efficiency generally decreases as the RE penetration increases and a larger amount of power flows through the energy storage system. With 81% round-trip efficiency, the storage system losses are the main source of inefficiency in the system. For moderate and large storage power capacities, generating electricity from a wind-wave mixture or pure wave increases the efficiency compared to pure wind because less power flows through the storage system.

The gas plant power fluctuation ratio shown in Fig. 8 is calculated as [71],

$$R_{\text{pr,gas}} = \frac{\text{Max}(P_G) - \text{Min}(P_G)}{\text{Mean}(P_G)}, \quad (6)$$

where P_G is the hourly power provided by the gas plant throughout the year. For increasing RE penetration levels, the gas plant power fluctuation generally increases and the gas plant capacity factor generally decreases. For 50% and 75% RE penetration, there is a band around 75% wave power with slightly less gas plant power fluctuation and higher gas plant capacity factor. This corresponds to a smaller coefficient of variation in the the renewable energy supply for wave power fractions of 70% and higher seen in Fig. A.11 in Appendix A.

As described in Section 5, the optimization procedure did not set the energy storage capacity, but permitted it to grow as required during the energy schedule optimization. As expected, larger RE penetration and larger storage power capacity benefit from larger energy storage capacity. This reflects how energy storage helps match the volatile wind and wave power sources with the relatively smooth power demand. For 50% RE penetration, the optimal energy storage capacity is approximately 20 h at the peak demand. For 100% RE penetration, the optimal energy storage capacity is 100–200 h at peak demand, or

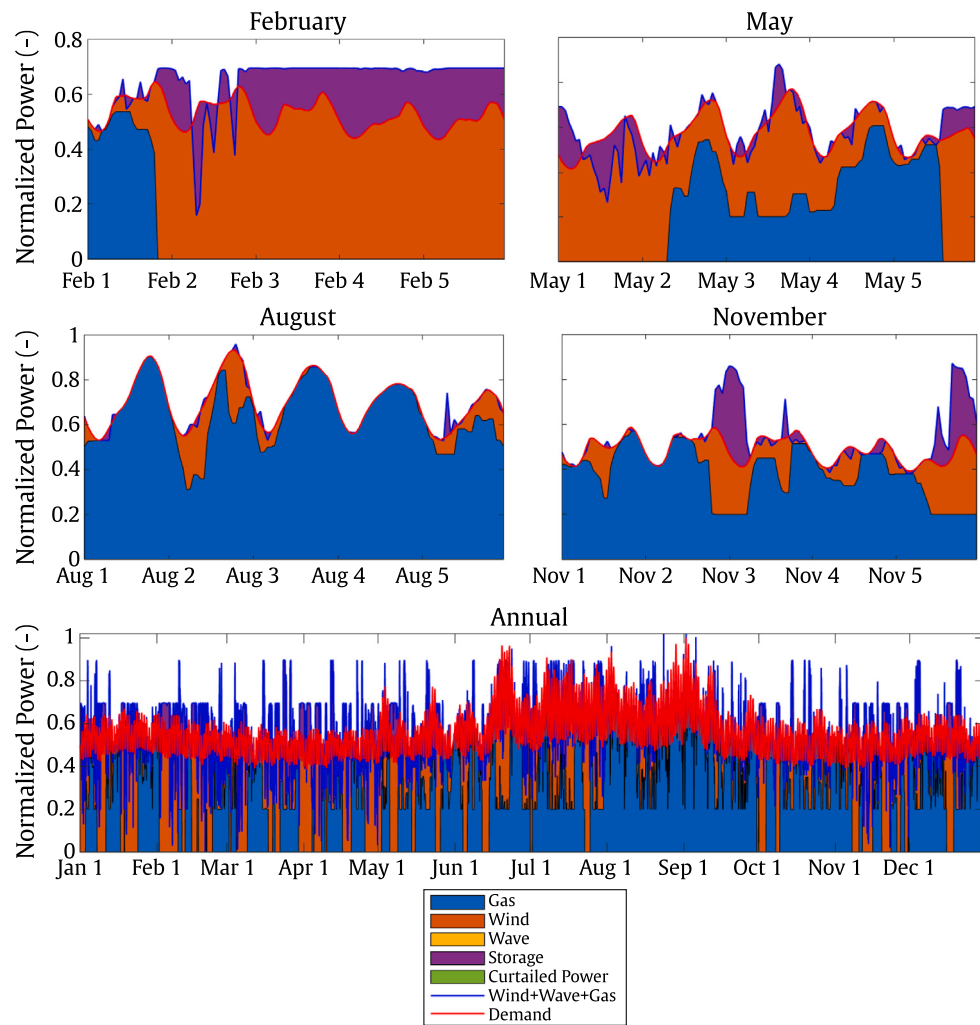


Fig. B.12. Simulated power balancing versus time for 50% RE penetration, 0% RE from wave power (100% RE from wind power), and power storage capacity at 50% of peak demand.

5–10 times larger. For 100% RE penetration and 75% storage power capacity, a 50%–50% wind-wave farm requires more energy storage than a differently split wind-wave farm.

The storage power capacity factor is the mean power flow in both directions through the storage system normalized by the storage system power capacity. As the RE penetration increases, the storage capacity factor generally increases, as is expected to match power demand. For all three RE penetration levels, increasing the fraction of wave power generally decreases the storage capacity factor. This corresponds to wave power requiring less smoothing than wind power to match power demand since wave power is less volatile.

7. Discussion

The overall goal of this paper was to investigate the role of wave energy converters and energy storage as grid renewable energy penetration increases. We hypothesized that co-locating wind and wave power would decrease the need for energy storage, and this benefit would magnify as the RE penetration increases because then RE smoothing becomes more critical to demand matching. Although the cost of wave power currently far exceeds the cost of wind power, we hypothesized that we would be able to identify promising power-balancing trends that can be leveraged in the future if the cost of wave power decreases as the wave industry matures. A unique approach of this study is that we simultaneously performed a parameter sweep of the wind-wave RE

fraction and energy storage power capacity and an optimization of the energy storage schedule in order to compare optimized trends in system performance.

The results confirm that a co-located wind-wave farm has smoother power supply, slightly less energy curtailment and slightly higher farm-to-grid efficiency than a solely wind farm. As described in Appendix A, a 100% wind farm has an annual power coefficient of variation (CoV) of 95% while incorporating 50% or more of wave power into the farm decreases the CoV to 79%. When RE penetration is 100% and storage power capacity equals 50% of peak demand, a farm with 50%–50% wave power decreases curtailed power by 3%–6%. When RE penetration is 100% and storage power capacity equals 100% of demand, a farm with 50%–50% wave power increases the electricity-grid efficiency by 2%–3%. This study found that incorporating wave power into the farm has negligible effect on the required amount of storage system energy capacity and gas plant power ramping. The benefits from wave power are generally more significant as the renewable energy penetration increases.

This study built on previous studies that considered power supply-demand matching strategies on the hourly scale for large renewable energy penetration levels [1,4,5,7]. These studies found that there was good potential for cost benefits from combining or co-locating wind and wave machines, although the wave power sector needs to develop further for wave power to be economically competitive with wind. Furthermore, these studies found that supply–demand matching with

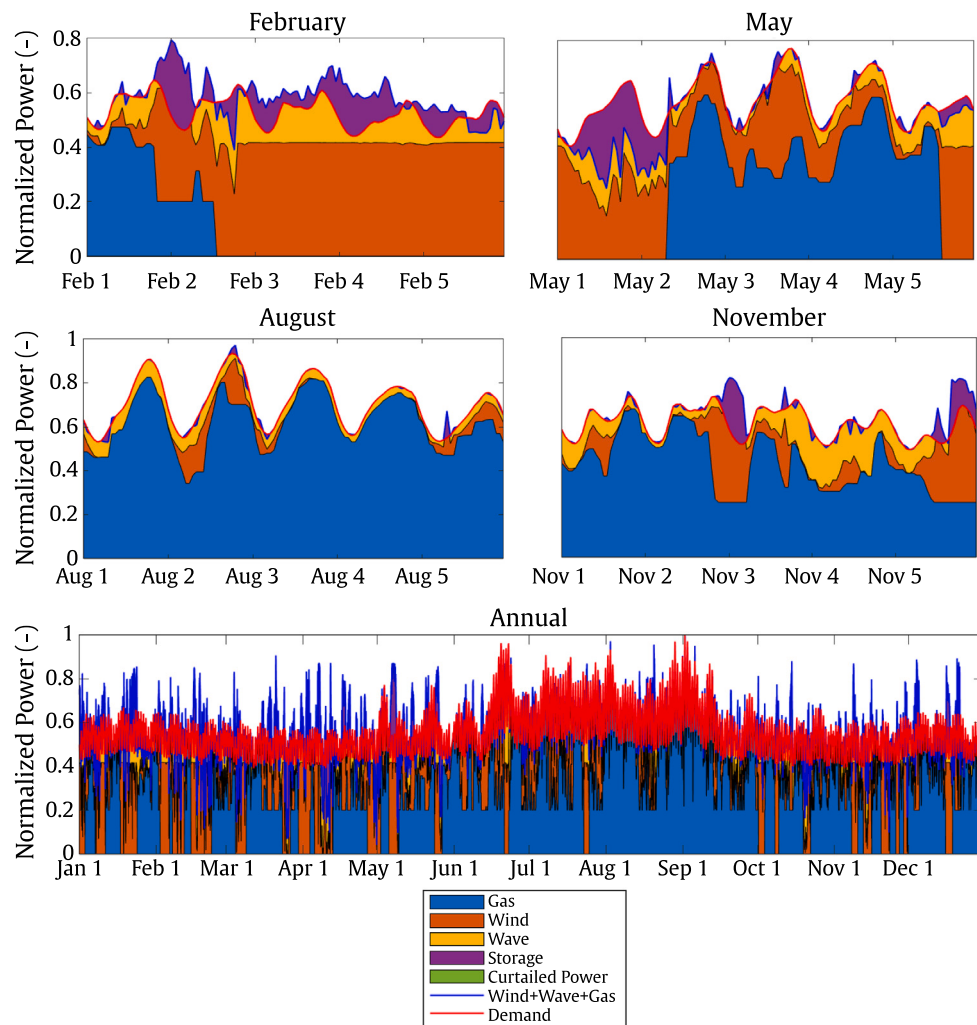


Fig. B.13. Simulated power balancing versus time for 50% RE penetration, 50% RE from wave power (50% RE from wind power), and power storage capacity at 50% of peak demand.

high RE penetration is feasible when the RE is supplemented by flexible conventional generation sources and energy storage, and the RE sources are diversified in both type and location. When relying on diversified locations, new cross-regional transmission lines are needed to provide sufficient grid connectivity, which increases RE cost.

The findings of this study agree with previous findings about the power smoothing trends for varied amounts of wind power, wave power, and energy storage. Astariz and Iglesias [4] found that there is an optimal combination of wind and wave power that minimizes the coefficient of variation (CoV) in the renewable energy power supply. This optimal combination level depends on the offshore site: a 50%–50% wind-wave split minimizes THD at one North Sea site while a 100%–0% wind-wave split minimizes CoV at another North Sea site. In Astariz and Iglesias's study, varying the wind-wave split varies the CoV by up to 13%. This 13% CoV is similar to the 16% CoV found by this study in [Appendix A](#).

Mai et al. [5] predicts that 7% of renewable power will be curtailed when RE penetration is 90% and power storage capacity is 9% of peak power demand. Cleary et al. [72] predicts that 4% of renewable power will be curtailed when RE penetration is 35% and power storage capacity is 2% of peak power demand. On the other hand, this study predicts that approximately 7% of the renewable power will be curtailed when the RE penetration is 50% (or 100%) and the power storage capacity is approximately 8% (or 63%) of peak power demand. This study requires a much larger energy storage capacity than [5] because [5] diversifies

the RE power among six different renewable resources and across all regions of the continuous United States. Similarly, this study requires a larger energy storage capacity than [72] because [72] uses a more varied portfolio of different renewable resources.

This study has several limitations that may be expanded as part of future research. First, this study is based on spar-platform FWTs and heave-mode point-absorber WECs. Different FWT and WEC designs will affect the cost and power trends. Different WEC designs have significantly different power performance while different FWT platform and WEC designs have significantly different costs [15,16,19,26]. Future research directions may investigate the benefits and sensitivity of the results to lower-cost WECs. Additionally, this study neglects how power spatial variability such as local wind gusts and 2D wave spectra and temporal variability on time scales less than an hour may affect the power supply–demand matching performance. Another limitation is lack of uncertainty propagation from wave-to-wire in the power and cost estimates. Future research may consider imperfect forecasting of the RE supply and power demand and different energy storage strategies. Furthermore, this study may be missing the effects of relatively rare extreme events that occur only once every several years. Future work may expand the parametric study to additional years to consider these events. Future research directions may also include investigating grids with renewable energy spread across different regions.

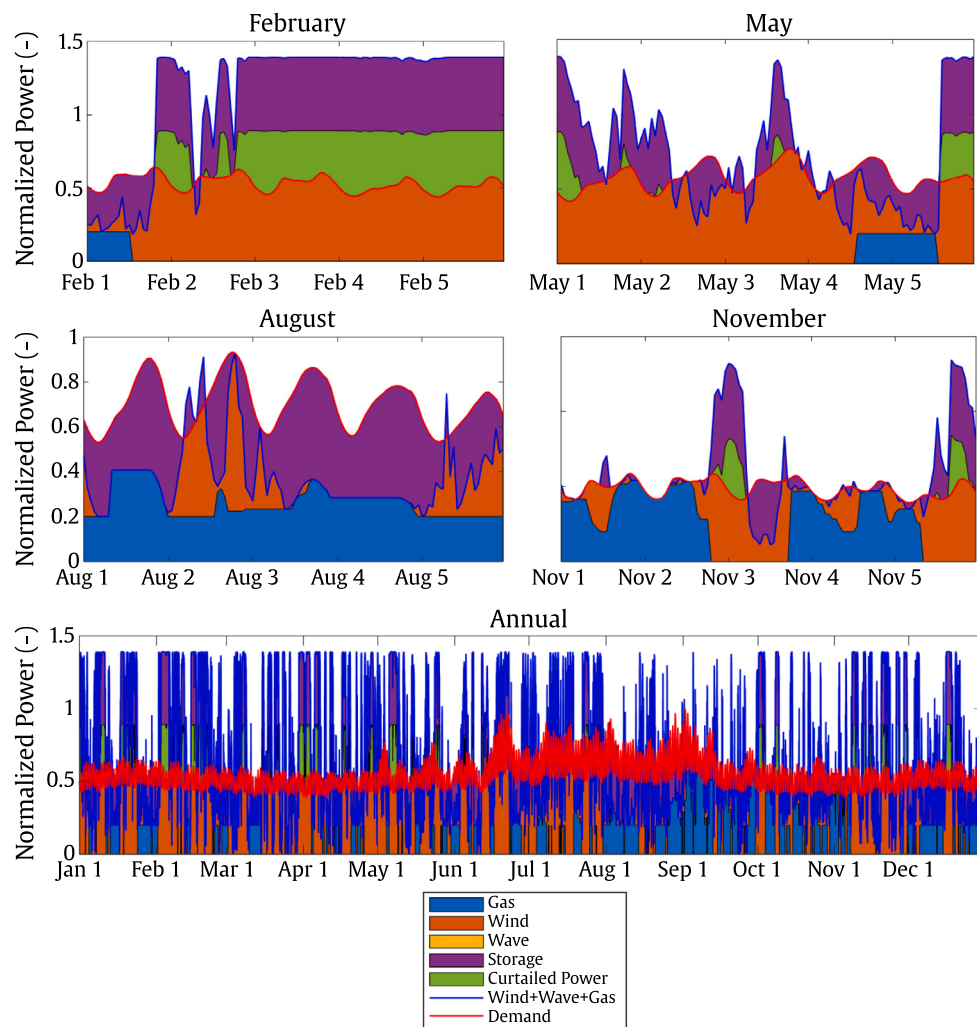


Fig. B.14. Simulated power balancing versus time for 100% RE penetration, 0% RE from wave power (100% RE from wind power), and power storage capacity at 50% of peak demand.

8. Conclusions

This paper found that for an electric grid comprised of 100% renewable energy, a hybrid 50%–50% wave-wind farm has the potential to decrease the farm power coefficient of variation by 16%, decrease power curtailment by 7%, and increase grid efficiency by 2% compared to a 100% wind farm. Varying the wind-wave fraction has a negligible effect on the required amount of storage system energy capacity and gas plant power ramping, performance metrics that are more sensitive to the storage power capacity. Remaining knowledge gaps and areas for future research concern the impact of different energy storage control algorithms, how to optimize the structures and control algorithms of a WEC attached to a FWT, how to decrease the cost of wave power so that it is more competitive with wind power, the impact of spatial variability in wind and wave characteristics across the farm, and uncertainty propagation in the cost and power models. The intent of this paper is to provide technical information to guide future researchers and policy makers in making decisions about offshore hybrid wind-wave-storage farms.

CRediT authorship contribution statement

Jocelyn M. Kluger: Conceptualization, Methodology, Software, Formal analysis, Data curation, Writing – original draft, Writing – review & editing, Visualization. **Maha N. Haji:** Conceptualization,

Methodology, Software, Formal analysis, Data curation, Writing – original draft, Writing – review & editing, Visualization. **Alexander H. Slocum:** Conceptualization, Writing – review.

Declaration of competing interest

The authors declare that they have no known competing financial interests or personal relationships that could have appeared to influence the work reported in this paper.

Data availability

Data will be made available on request.

Appendix A. Correlations of wind, wave, and demand

It is well known that diversifying the type of renewable energy sources can smooth the aggregate renewable energy power supply [5]. This is generally always beneficial for matching supply and demand since the renewable energy power supply is much more variable than the demand.

The wind, wave, and demand data for the Eureka, California region in 2017 confirm that the wind and wave power supplies are much more variable than the demand. The wind and wave power are uncorrelated enough that combining them can smooth out the aggregate supply. Wave power is generally less variable than wind power.

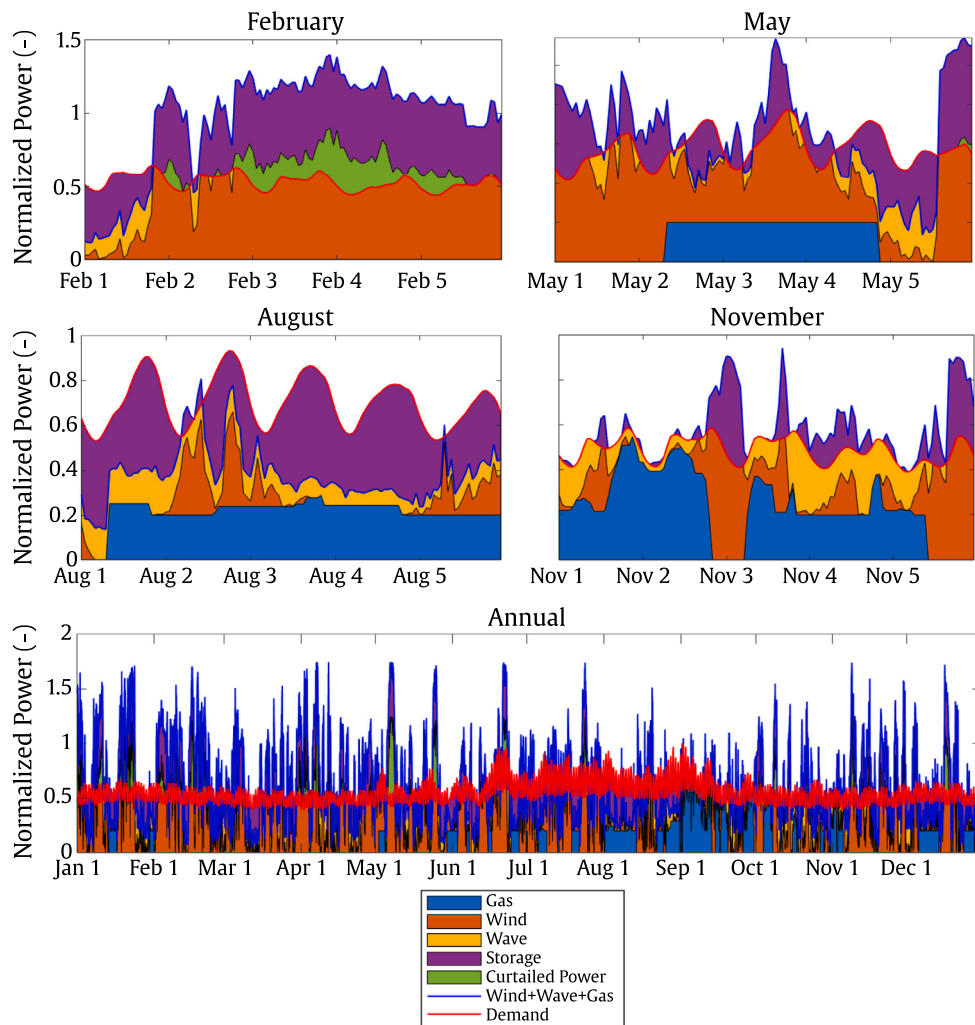


Fig. B.15. Simulated power balancing versus time for 100% RE penetration, 50% RE from wave power (50% RE from wind power), and power storage capacity at 50% of peak demand.

Fig. A.10 plots time series of the Eureka power data that is normalized so each power has an annual maximum value of 1. The demand data is based on hourly data provided by CAISO for the PGE region throughout 2017. The wind and wave power data is based on the wind turbine and WEC power curves for hourly wind speeds and sea states, as described in Sections 2.1 and 2.2, respectively.

Fig. A.11 compares the coefficient of variation of farms with different power distributions of wind and wave,

$$CoV = \frac{\text{Standard Deviation in power}}{\text{Mean power}}. \quad (\text{A.1})$$

Smaller *CoV* is an indicator of smoother power. The most significant annual smoothing occurs when a farm's composition is changed from 100% wind (0% wave) to 50% wind (50% wave). This decreases the annual *CoV* from 95% to 79% (16% decrease). Further increases in the fraction of wave power does not significantly decrease the annual *CoV*, but it does significantly decrease the *CoV* over shorter time periods in some seasons. The smoothing effects are more pronounced in the summer (August) and Autumn (November) seasons.

Due to the present significantly higher cost of wave power compared to wind power, a farm with 50% wave power might not be economically feasible without further WEC innovation. Given this limitation, it is promising that **Fig. A.11** shows that changing the farm from 100% wind (0% wave) to just 90% wind (10% wave) decreases the annual coefficient of variation from 95% to 90% (5% decrease). This distribution might be more economically feasible and potentially significantly

improve the system supply–demand balancing. A hypothesis of this study is that the smoothing effects of diversified renewable energy sources may decrease the required energy storage capacity and gas plant ramping necessary to make the intermittent RE power supply match the much smoother power demand.

Appendix B. Time series results for key parameter sets

Figs. B.12–B.13 provide more detail on the optimized supply–demand balancing at various renewable energy penetration levels and wind-wave renewable energy fractions for the isolated-grid shoreline community. All figures fix the power storage capacity at 50% of peak demand. The power values of the y-axis have been normalized by the annual peak demand power.

References

- [1] Georgilakis P. Technical challenges associated with the integration of wind power into power systems. *Renew Sustain Energy Rev* 2008;12:852–63.
- [2] Fusco F, Nolan G, Ringwood JV. Variability reduction through optimal combination of wind/wave resources—An Irish case study. *Energy* 2010;35(1):314–25.
- [3] Stoutenburg ED, Jacobson MZ. Reducing offshore transmission requirements by combining offshore wind and wave farms. *IEEE J Ocean Eng* 2011;36(4):552–61.
- [4] Astariz S, Iglesias G. Output power smoothing and reduced downtime period by combined wind and wave energy farms. *Energy* 2016;97:69–81.

- [5] Mai T, Wiser R, Sandor D, Brinkman G, Heath G, Denholm P, et al. Exploration of high-penetration renewable electricity futures. Vol. 1 of renewable electricity futures study. Technical report, National Renewable Energy Laboratory; 2012.
- [6] Sangster AJ. Massive energy storage systems enable secure electricity supply from renewables. *J Mod Power Syst Clean Energy* 2016;4(4):659–67.
- [7] Díaz-González F, Sumper A, Gomis-Bellmunt O, Villafáfila-Robles R. A review of energy storage technologies for wind power applications. *Renew Sustain Energy Rev* 2012;16(4):2154–71.
- [8] Schwartz M, Heimiller D, Haymes S, Musial W. Assessment of offshore wind energy resources for the United States. Technical report, National Renewable Energy Laboratory (NREL); 2010.
- [9] Matha D. Model development and loads analysis of a wind turbine on a floating offshore tension leg platform [Master's thesis], University of Colorado, Boulder; 2009.
- [10] Butterfield S, Musial W, Jonkman J, Sclavounos P, Wayman L. Engineering challenges for floating offshore wind turbines. *Proc Cph Offshore Wind Conf* 2005.
- [11] Sebastian T, Lackner M. Characterization of the unsteady aerodynamics of offshore floating wind turbines. *Wind Energy* 2013;16:339–52.
- [12] Tran T, Kim D. The platform pitching motion of floating offshore wind turbine: A preliminary unsteady aerodynamic analysis. *J Wind Eng Ind Aerodyn* 2015;142:65–81.
- [13] Myhr A, Bjerkseter C, Ågtnes A, Nygaard TA. Levelised cost of energy for offshore floating wind turbines in a life cycle perspective. *Renew Energy* 2014;66:714–28.
- [14] Roddier D, Cermelli C, Aubault A, Weinstein A. WindFloat: A floating foundation for offshore wind turbines. *J Renew Sustain Energy* 2010;2(3):033104.
- [15] Jonkman J. Definition of the floating system for phase IV of OC3. Technical report TP-500-47535, U.S. Department of Energy; 2010.
- [16] Stehly T, Beiter P, Duffy P. 2019 cost of wind energy review. Technical report TP-5000-78471, National Renewable Energy Laboratory; 2020.
- [17] Gao Z-t, Feng X-y, Zhang Z-t, Liu Z-l, Gao X-x, Zhang L-j, et al. A brief discussion on offshore wind turbine hydrodynamics problem. *J Hydraul* 2022;34(1):15–30.
- [18] Karimirad M. Offshore energy structures: For wind power, wave energy and hybrid marine platforms. Springer; 2014.
- [19] Robertson AN, Jonkman JM. Loads analysis of several offshore floating wind turbine concepts. In: The twenty-first international offshore and polar engineering conference. OnePetro; 2011.
- [20] Robertson A, Jonkman J, Masciola M, Song H, Goupee A, Coulling A, et al. Definition of the semisubmersible floating system for phase II of OC4. Technical report, Golden, CO, United States: National Renewable Energy Lab. (NREL); 2014.
- [21] Neary V, Previsic M, Jepsen R, Lawson M, Yu Y, Copping A, et al. Methodology for design and economic analysis of Marine Energy Conversion (MEC) technologies. Technical report, Sandia National Laboratories; 2014.
- [22] Baca E, Philip RT, Greene D, Battey H. Expert elicitation for wave energy LCOE futures. Technical report, Golden, CO, United States: National Renewable Energy Lab.(NREL); 2022.
- [23] Reikard G, Robertson B, Bidlot J. Combining wave energy with wind and solar: Short-term forecasting. *Renew Energy* 2015;81:442–56.
- [24] Kluger J. Synergistic design of a combined floating wind turbine - wave energy converter [Ph.D. thesis], Massachusetts Institute of Technology; 2017.
- [25] Falnes J, Hals J. Heaving buoys, point absorbers and arrays. *Phil Trans R Soc A* 2012;370(1959):246–77.
- [26] Drew B, Plummer AR, Sahinkaya MN. A review of wave energy converter technology. London, England: Sage Publications Sage UK; 2009.
- [27] Barrios IM, Lynch K, Murphy J, Pavon CL. Methodology for assessing multiple combined wind and ocean energy technologies as part of the EU FP7 MARINA platform project. In: Proceedings of 4th international conference on ocean energy. 2012.
- [28] Serri I, Sempreviva A, Pontes T, Murphy J, Lynch K, Airoldi D, et al. Resource data and GIS tool for offshore renewable energy projects in Europe. Technical report, ORECCA; 2012.
- [29] Casale C, Serri I, Stolk N, Yıldız I, Cantú M. Synergies, innovative designs and concepts for multipurpose use of conversion platforms. Results of ORECCA project-WP4. Technical report, ORECCA; 2012.
- [30] Jeffrey H, Sedgwick J. European offshore renewable energy roadmap. Technical report, ORECCA; 2011.
- [31] Yu Y-H, Jenne D, Thresher R, Copping A, Geerlofs S, Hanna LA. Reference model 5 (RM5): Oscillating surge wave energy converter, NREL/TP-5000-62861. Technical report, National Renewable Energy Laboratory; 2015.
- [32] Astariz S, Iglesias G. The economics of wave energy: a review. *Renew Sustain Energy Rev* 2015;45:397–408.
- [33] Clark CE, Miller A, DuPont B. An analytical cost model for co-located floating wind-wave energy arrays. *Renew Energy* 2019;132:885–97.
- [34] Pecher A. Handbook of ocean wave energy. Springer; 2017.
- [35] Copping A, Geerlofs S. The contribution of environmental siting and permitting requirements to the cost of energy for marine and hydrokinetic devices. Technical report, Pacific Northwest National Laboratory; 2011.
- [36] Mulianwan M, Karimirad M, Moan T. Dynamic response and power performance of a combined spar-type floating wind turbine and coaxial floating wave energy converter. *Renew Energy* 2013;50:47–57.
- [37] Haji MN, Kluger JK, Sapsis TP, Slocum AH. A symbiotic approach to the design of offshore wind turbines with other energy harvesting systems. *Ocean Eng* 2018;169:673–81.
- [38] Experimental and numerical investigations of a two-body floating-point absorber wave energy converter in regular waves. *J Fluids Struct* 2019;91:102613.
- [39] Mei C. Hydrodynamic principles of wave power extraction. *Philos Trans R Soc* 2012;370:208–34.
- [40] Hals J, Falnes J, Moan T. Constrained Optimal Control of a Heaving Buoy Wave-Energy Converter. *J Offshore Mech Arct Eng* 2010;133(1).
- [41] Pérez-Collazo C, Greaves D, Iglesias G. A review of combined wave and offshore wind energy. *Renew Sustain Energy Rev* 2015;42:141–53.
- [42] da Silva L, Sergienko N, Cazzolato B, Ding B. Dynamics of hybrid offshore renewable energy platforms: Heaving point absorbers connected to a semi-submersible floating offshore wind turbine. *Renew Energy* 2022;199:1424–39.
- [43] Gao Z, Moan T, Wan L, Michailides C. Comparative numerical and experimental study of two combined wind and wave energy concepts. *J Ocean Eng Sci* 2016;1(1):36–51.
- [44] Wang Y, Shi W, Michailides C, Wan L, Kim H, Li X. WEC shape effect on the motion response and power performance of a combined wind-wave energy converter. *Ocean Eng* 2022;250:111038.
- [45] Snyder B, Kaiser MJ. Ecological and economic cost-benefit analysis of offshore wind energy. *Renew Energy* 2009;34(6):1567–78.
- [46] Westerberg V, Jacobsen JB, Lifran R. The case for offshore wind farms, artificial reefs and sustainable tourism in the French mediterranean. *Tour Manag* 2013;34:172–83.
- [47] Galparsoro I, Menchaca I, Garmendia JM, Borja Á, Maldonado AD, Iglesias G, et al. Reviewing the ecological impacts of offshore wind farms. *Npj Ocean Sustain* 2022;1(1):1–8.
- [48] Succar S, Williams R. Compressed air energy storage: Theory, resources, and applications for wind power. Technical report, Princeton Environmental Institute Report No. 8; 2008.
- [49] Staffell I. Wind turbine power curves. Technical report, Imperial College; 2012.
- [50] Fingersh L, Hand M, Laxson A. Wind turbine design cost and scaling model. Technical report, National Renewable Energy Laboratory (NREL); 2006.
- [51] Elliot DL, Holladay CG, Barchet WR, Foote HP, Sandusky WF. Wind energy resource atlas of the United States. 1987.
- [52] Marean JB. Compressed air energy storage engineering and technical study. Technical report, Albany: New York State Energy Research and Development Authority; 2009.
- [53] EPRI-DOE handbook of energy storage for transmission and distribution applications. Technical report, U.S. Department of Energy; 2003.
- [54] Schoenung S, Hassenzahl WV. Long- vs. Short-term energy storage technologies analysis. Technical report, Sandia National Laboratories; 2003.
- [55] King M, Jain A, Bhakar R, Mathur J, Wang J. Overview of current compressed air energy storage projects and analysis of the potential underground storage capacity in India and the UK. *Renew Sustain Energy Rev* 2021;139:110705.
- [56] Van den Bergh K, Delarue E. Cycling of conventional power plants: technical limits and actual costs. Technical report WP EN2015-5, KULeuven Energy Institute TME Branch; 2015.
- [57] Zoellick J. Humboldt County general plan 2025 energy element background technical report. Technical report, Schatz Energy Research Center, Humboldt State University; 2005.
- [58] Todorovic J. Loss evaluation of HVAC connection of large offshore wind farms [Master's thesis], KTH Royal Institute of Technology; 2004.
- [59] Ackermann T, Negra NB, Todorovic J, Lazaridis LP. Evaluation of electrical transmission concepts for large offshore windfarms. *Proc Cph Offshore Wind* 2005;1–10.
- [60] Daniel JP, Liu S, Ibanez E, Pennock K, Reed G, Hanes S. National offshore wind energy grid interconnection study executive summary. Technical report, 2014.
- [61] Beiter P, Musial W, Smith A, Kilcher L, Damiani R, Maness M, et al. A spatial-economic cost-reduction pathway analysis for U.S. offshore wind energy development from 2015–2030. Technical report, National Renewable Energy Laboratory; 2016.
- [62] Brakelmann H. Efficiency of HVAC power transmission from offshore-windmills to the grid. In: IEEE Bologna powertech conference. 2003.
- [63] Negra NB, Todorovic J, Ackermann T. Loss evaluation of HVAC and HVDC transmission solutions for large offshore wind farms. *Electr Power Syst Res* 2006;11:916–27.
- [64] Denholm P, Kulcinski G. Life cycle energy requirements and greenhouse gas emissions from large scale energy storage systems. *Energy Convers Manage* 2004;45:2153–72.
- [65] Zakeri B, Syri S. Electrical energy storage systems: A comparative life cycle cost analysis. *Renew Sustain Energy Rev* 2015;42:569–96.
- [66] Liu M, Quilumba FL, Lee W-J. Dispatch scheduling for a wind farm with hybrid energy storage based on wind and LMP forecasting. *IEEE Trans Ind Appl* 2015;51(3):1970–7.

- [67] Impram S, Nese S, Oral B. Challenges of renewable energy penetration on power system flexibility: A survey. *Energy Strategy Rev* 2020;31:100539.
- [68] Barton J, Infield D. Energy storage and its use with intermittent renewable energy. *IEEE Trans Energy Convers* 2004;19(2):441–8.
- [69] Damiano A, Gatto G, Marongiu I, Porru M, Serpi A. Real-time control strategy of energy storage systems for renewable energy sources exploitation. *IEEE Trans Sustain Energy* 2013;5(2):567–76.
- [70] LeCun Y, Bengio Y, Hinton G. Deep learning. *Nature* 2015;521(7553):436–44.
- [71] Stefek J, Bain D, Yu Y, Jenne D, Stark G. Analysis on the influence of an energy storage system and its impact to the grid for a wave energy converter. In: *Proceedings of the ASME 2019 38th international conference on ocean, offshore, and arctice engineering*. 2019.
- [72] Cleary B, Duffy A, OConnor A, Conlon M, Fthenakis V. Assessing the economic benefits of compressed air energy storage for mitigating wind curtailment. *IEEE Trans Sustain Energy* 2015;6(3):1021–8.